Supporting Information

Metal-free Electrocatalysts for Efficient Oxygen Reduction Reaction Based on Covalent Organic Frameworks with Linker Polar Modulation

Table of Content

Section 1. Materials and methods

1.1 Materials

p-Nitrobenzaldehyde, $SnCl_2 \cdot 2H_2O$, pyrrole, 4,4'-Biphenyldicarboxaldehyde (BDC), 2,2'-Bipyridyl-5,5'-dialdehyde (BPY), benzyl alcohol, 1,2-dichlorobenzene, *n*-butanol and acetic acid were obtained from Aladdin Industrial Corporation (Shanghai, China). Acetic anhydride, propionic acid, acetone, pyridine, ammonia water, Hydrogen chloride solution (HCl) and chloroform were purchased from the Damao chemical reagent factory (Tianjin, China). The purchased chemical materials listed below were used without any additional purification.

1.2 Material characterizations

The equipment used to do the characterization work is as listed below: X-ray diffraction (XRD) was performed on a Rigaku D/MAX-2500 diffractometer with Cu Kα radiation (λ=1.5406 Å). Solid ultraviolet (UV) spectra were recorded using a UV–vis Spectrometer Lambda 750S (Perkin Elmer, Inc., USA) at room temperature. Fourier transform infrared (FT–IR) spectra were recorded using a Thermo Scientific Nicolet iS10 spectrometer. Transmission electron microscope (TEM) and high-resolution TEM images were recorded on a transmission electron microscope (JEOL, JEM–2100). X-ray photoelectron spectroscopy (XPS) data were collected using a Thermo Scientific K-Alpha spectrometer. Nitrogen adsorption/desorption isotherms were obtained on a Quantachrome Autosorb iQ apparatus at 77 K. The specific surface areas were calculated using the Brunauer Emmett–Teller (BET) method. The samples were degassed at 120 °C for 12 h before measurements were taken.

Section 2. Synthetic Procedures

2.1 Synthesis of 5,10, 15, 20-tetrakis (4-aminophenyl)-21*H*,23*H*-porphyrin:

Following a modified procedure from reference.[1]

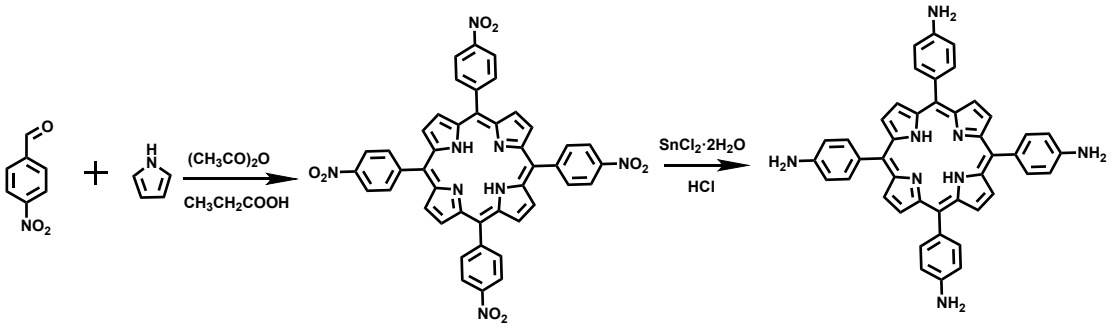

2.2 Synthesis of 5,10,15,20-tetrakis (4-nitrophenyl)-21H,23*H*-porphyrin(TNPP):

In a 500 mL flask, p-Nitrobenzaldehyde (11 g, 0.07 mol), propionic acid (300 mL) and acetic anhydride (12 mL) were added and heat to 125 °C to reflux with stirring. Then the mixed solution with 5 mL of pyrrole and 10 mL of propionic acid was added and continue refluxing under stirring for 1h. After that the mixed solution was cooled to room temperature and placed in the refrigerator for 24 h. Then the crude product was affording through vacuum filtered, then washed with water for several times. Put the crude product in 70 °C vacuum oven for overnight to drying to obtain purple-black solid. After that, the solid was mixed with 80 mL of pyridine and refluxed for 1 h, then cooled to room temperature and stored at -4 °C overnight to get black precipitate. Then the solvent was removed through vacuum filtered and washed the filter cake with acetone for several times until the filtrate become colorless, yielding bright purple product TNPP.

2.3 Synthesis of 5,10,15,20-tetrakis(4-aminophenyl)-21*H*,23*H*-porphyrin (TAPP):

The second step is the reduction of nitro to amino groups. 2 g of TNPP was dissolved in 100 mL of concentrated hydrochloric acid. 25 mL of concentrated hydrochloric acid solution containing 9 g of $SnCl_2 \cdot 2H_2O$ was added dropwise to the porphyrin solution within 10 min at room temperature under stirring, and then the temperature was raised to 70 °C for 2.5h. The mixture was cooled to room temperature and filtered to obtain a dark green solid, which was dispersed in 200 mL of deionized water. The pH was adjusted to 9 using concentrated ammonia, and the mixture was filtered again to collect the filter cake. The filter cake was then added to 200 mL of a 5% NaOH solution, ultrasonically stirred until uniform, and filtered once more. The solid was washed several times with deionized water and vacuum-dried at 70°C. The

resulting product was subjected to Soxhlet extraction using 300 mL of chloroform, and the solvent was concentrated by rotary evaporation to yield bright purple porphyrin crystals. ^{1}H NMR (500 MHz, DMSO-d6) δ 8.88 (s, 8H), 7.84 (s, 8H), 6.99 (s, 8H), 5.56 (s, 8H), -2.73 (s, 2H).

2.4 Synthesis of TAPP-COF$_{BDC}$

The porphyrin-based TAPP-COF$_{BDC}$ was synthesized according to a previously reported method[2]. A Pyrex tube was charged with 5,10,15,20-Tetrakis(4-aminophenyl)-21*H*,23*H*-porphyrin (TAPP, 16.9 mg, 0.05 mmol), 4,4'-Biphenyldicarboxaldehyde (BDC, 10.5 mg, 0.10 mmol), 0.75 mL 1,2-dichlorobenzene and 0.25 mL *n*-butanol, and then the mixture was sonicated for 10 min. Upon the addition of aqueous acetic acid (3 M, 0.2 mL), the solution underwent an additional 5 minutes of sonication to ensure even dispersion. Afterwards, the tube was flash frozen in a liquid nitrogen bath and degassed by three freeze-pump-thaw cycles, sealed under vacuum, and heated at 120 ºC for 3 days. After cooling down to room temperature, the tube was open and the resulting precipitate was filtered off, thoroughly washed DMF, THF and acetone until the filtrate was colorless, and Soxhlet extractions with THF for 24 h, respectively. Finally, the resulting powder was dried under vacuum at 120 ºC overnight to produce TAPP-COF$_{BDC}$ as a purple solid (16.7 mg, 65% yield).

2.5 Synthesis of TAPP-COF$_{BPY}$

The TAPP-COF$_{BPY}$ was synthesized according to a previously reported protocol with a slight modification.[3] A Pyrex tube was charged with 5,10,15,20-Tetrakis(4-aminophenyl)-21*H*,23*H*-porphyrin (TAPP, 13.5 mg 0.02 mmol), 2,2'-Bipyridyl-5,5'-dialdehyde (BPY, 8.5 mg, 0.04 mmol), 0.75 mL benzyl alcohol and 0.25 mL 1,2-dichlorobenzene, and then the mixture was sonicated for 10 min. Upon the addition of aqueous acetic acid (6 M, 0.1 mL), the solution underwent an additional 5 minutes of sonication to ensure even dispersion. Afterwards, the tube was flash frozen in a liquid nitrogen bath and degassed by three freeze-pump-thaw cycles, sealed under vacuum, and heated at 120 ºC for 3 days. After cooling down to room temperature, the tube was open and the resulting precipitate was filtered off, thoroughly washed THF and acetone until the filtrate was colorless, and Soxhlet extractions with THF for 24 h, respectively.

Finally, the resulting powder was dried under vacuum at 120 ºC overnight to produce TAPP-COF_{BPY} as a purple solid (13.2 mg, 64% yield).

Section 3. Electrochemical measurements

The electrochemical tests were conducted on an RRDE on a CHI 760E workstation, coupled to an RRDE rotator: a glassy carbon disc electrode (Ø = 5.61 mm), a Pt ring electrode (Ø inner = 6.25 mm, Ø outer = 7.9 mm), a graphite rod was used as counter electrode and Ag/AgCl as reference electrode. Each catalyst (5 mg) was dispersed into 1 mL solution composed of 9: 10: 1 = ethanol: H_2O: Nafion (5 wt%) solution, and then the mixed solution was sonicated for 30 minutes. 10 μL ink was loaded onto the RRDE electrode and dried at 500 rpm. Before testing, the electrolyte was saturated with oxygen by continuously passing oxygen through the 0.1 M KOH electrolyte for 30 minutes. Subsequently, a 30 cycles CV sweep (sweep rate 50 mV/s) was performed to activate the catalyst, with the oxygen continuously applied during the test. The catalyst was stabilized when the CV curve remained essentially unchanged. After the CV activation was completed, the test was suspended again and oxygen was added for 20 minutes to replenish the dissolved oxygen consumed during the CV test, and then the LSV test was performed. A linear voltage of 0.2 - -0.8 V vs. Ag/AgCl was applied to the disk electrode and 1.3 V vs. RHE was applied to the ring electrode, with a scan rate of 10 mV/s and a RRDE rotate speed at 400 - 1600 rpm. After 30 min of continuous nitrogen in the electrolyte, a CV scan was performed to test the background current in this system to verify that the reaction occurring in the system was an oxygen reduction reaction.

The H_2O_2 selectivity, electron-transfer number (n) and Faradaic efficiency (%) were calculated from the following function respectively:

$$H_2O_2\% = \frac{200 \times I_{ring}/N}{|I_{disk}| + I_{ring}/N} \quad \text{(S1)}$$

$$n = \frac{4|I_{disk}|}{|I_{disk}| + I_{ring}/N} \quad \text{(S2)}$$

$$Faradaic\ efficiency(\%) = \frac{100 \times I_{ring}}{|I_{disk}| \times N} \quad \text{(S3)}$$

where I_{disk} and I_{ring} are the disk current and ring current, and N stands for the current collection efficiency of the Pt ring, which is determined to be 0.37.

To aid in verifying the accuracy of the RRDE test, Koutecky-Levich plots were performed. By testing the disk current at 400 - 1600 rpm, the number of electrons transferred was calculated according to Equation S4 – S6.

$$\frac{1}{J} = \frac{1}{J_L} + \frac{1}{J_K} = \frac{1}{B\omega^{1/2}} + \frac{1}{J_K} \quad \text{(S4)}$$

$$J_K = nFkC_0 \quad \text{(S5)}$$

$$B = nFC_0 D_0^{2/3} v^{-1/6} \quad \text{(S6)}$$

Where J is the measured current density, J_K and J_L are the kinetic and limiting current densities, ω is the angular velocity, n is electron transfer number, F (96485 C mol^{-1}) is the Faraday constant, D_0 is the diffusion coefficient of O_2 in 0.1 M KOH (1.9×10^{-5} cm^2 s^{-1}), C_0 is the bulk concentration of O_2 (1.2×10^{-3} mol L^{-1}), v is the kinetic viscosity of the electrolyte (0.01 cm^2 s^{-1}), and k is the electron-transfer rate constant. Subsequently, the catalyst stability was tested by continuously passing oxygen for a period of time to saturate the solution with oxygen. The stability test was conducted at a low RRDE speed of 1600 rpm for a long period of time. A voltage of 0.6 V vs. RHE was applied to the disk electrode and a test voltage of 1.3 V vs. RHE was applied to the ring electrode.

H_2O_2 yield measurement: The H_2O_2 yield was measured by the Ce^{4+} titration method in an H-cell with Nafion 117 membrane as the separator. Carbon fiber paper (1 cm*1 cm) was employed as the working electrode loaded with catalysts (~ 0.1 mg cm^{-2}). Both of the compartments of the cell were filled with 20 ml electrolyte (0.1 M KOH). The Ce^{4+} titration method worked based on the following reaction.

$$2Ce^{4+} + H_2O_2 \rightarrow 2Ce^{3+} + 2H^+ + O_2 \quad \text{(S7)}$$

The yellow solution of Ce^{4+} would be reduced by H_2O_2 to colorless Ce^{3+}. Thus,

the concentration of H_2O_2 could be figured out by measuring the concentration of Ce^{4+} before and after the reaction via ultraviolet-visible spectroscopy. The concentration of H_2O_2 was calculated based on the following equation:

$$C_{H_2O_2} = \frac{1}{2}\Delta C_{Ce^{4+}} \quad \text{(S8)}$$

The linear calibration curve between Ce^{4+} concentration and absorbance at 316 nm (**Figure S9**) was established based on a series of $Ce(SO_4)_2$ solutions (0.05-0.6 mM). 1 mM $Ce(SO_4)_2$ solution was prepared by dissolving 33.2 mg $Ce(SO_4)_2$ in 100 ml 0.5 M H_2SO_4. The electrolytic droplet after a certain reaction time was placed in 3 mL 1 mM $Ce(SO_4)_2$ solution to make the yellow solution pale, and the volume of droplet adding electrolyte and the catalytic reaction time were recorded. By measuring the UV absorption of the diluted $Ce(SO_4)_2$, the concentration of H_2O_2 can be calculated from the above quantitative relationship.

Section 4. Supplementary figures

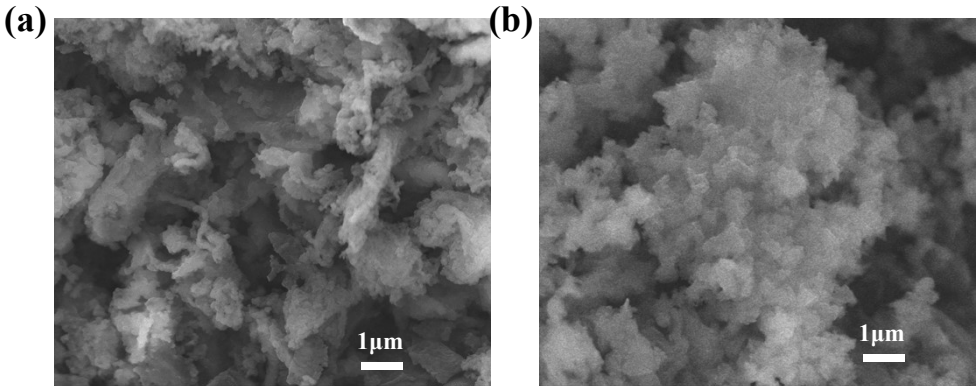

Figure S1. SEM images of TAPP-COF_{BDC} and TAPP-COF_{BPY}.

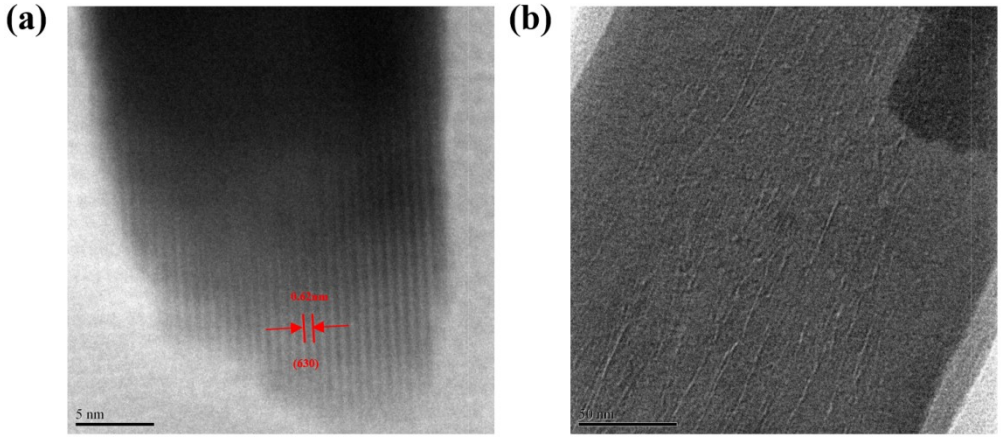

Figure S2. TEM images of (a) TAPP-COF_{BDC} and (b) TAPP-COF_{BPY}

Figure S2 presents the TEM images of TAPP-COF_{BDC} and TAPP-COF_{BPY}. TAPP-COF_{BDC} exhibits a lattice spacing of 0.62 nm corresponding to the (630) crystallographic plane. In contrast, TAPP-COF_{BPY} displays a lamellar morphology without observable lattice fringes. This phenomenon is likely attributed to electron beam-induced structural degradation (e.g., bond cleavage, framework collapse) during TEM imaging when exposed to the high-energy electron beam. Such irradiation effects may induce disordering in originally ordered crystalline domains, accompanied by the loss of long-range periodicity required for resolving lattice fringes (Micron, 2004, 35(6): 399-409). This radiation damage mechanism fundamentally obscures the crystallographic signatures in the acquired micrographs.

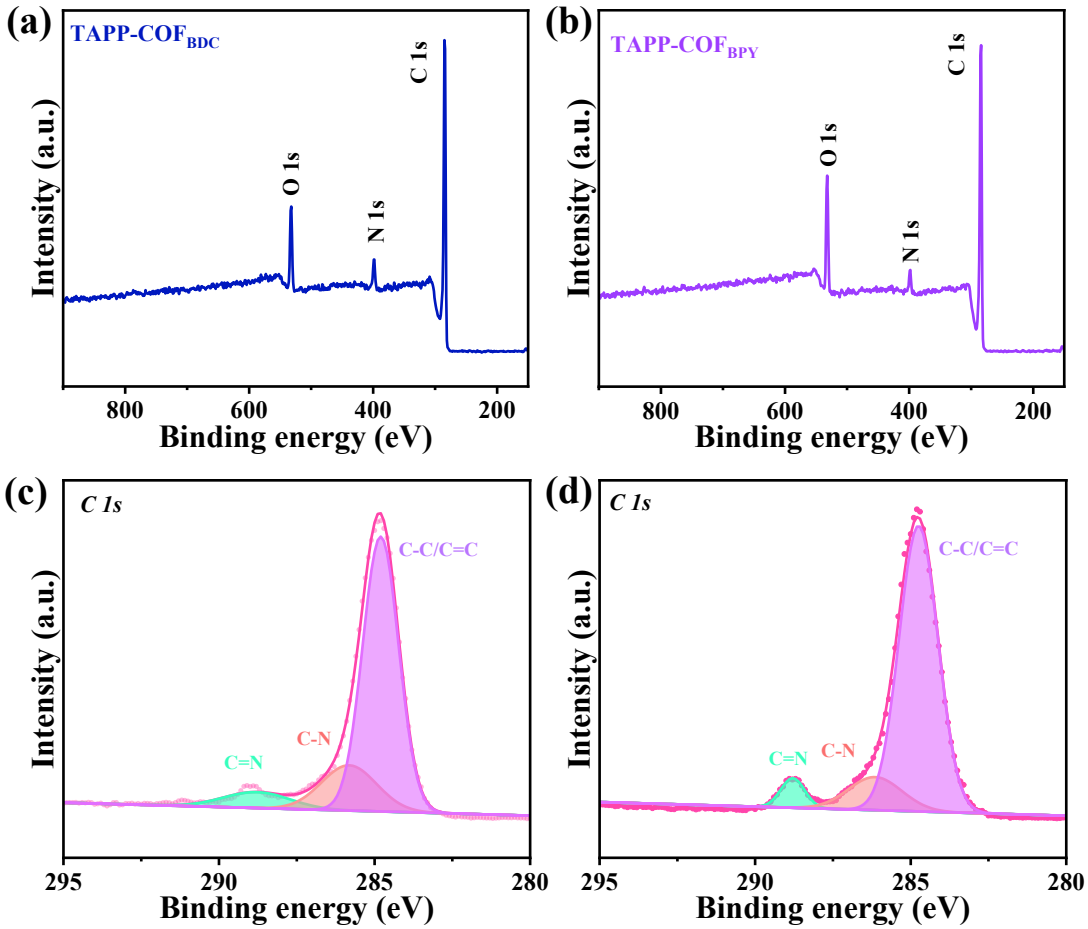

Figure S3. The XPS full spectra and XPS C 1*s* spectra of TAPP-COF$_{BDC}$ and TAPP-COF$_{BPY}$.

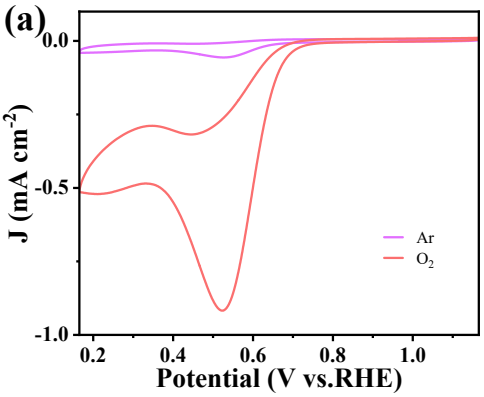

Figure S4. The CV plots of the TAPP-COF$_{BDC}$.

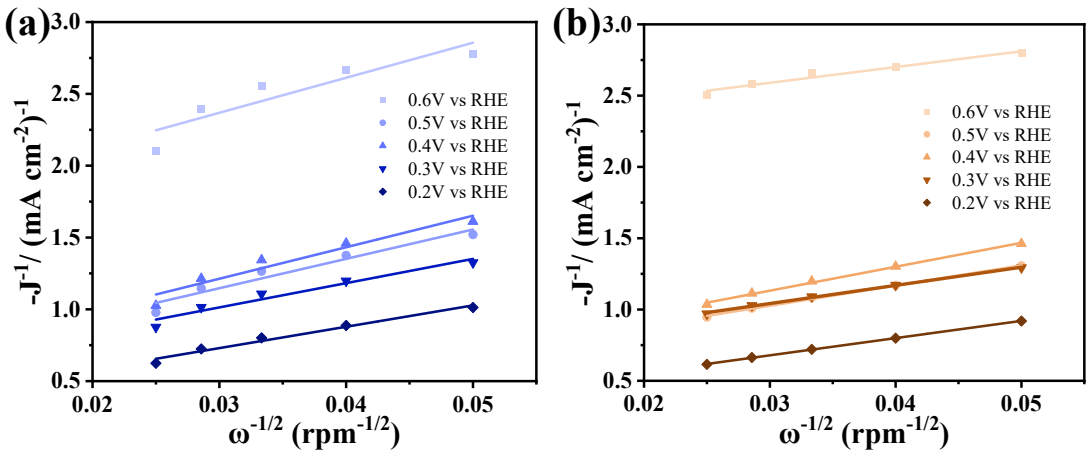

Figure S5. K–L plots of (a) TAPP-COF_{BDC} and (b) TAPP-COF_{BPY}.

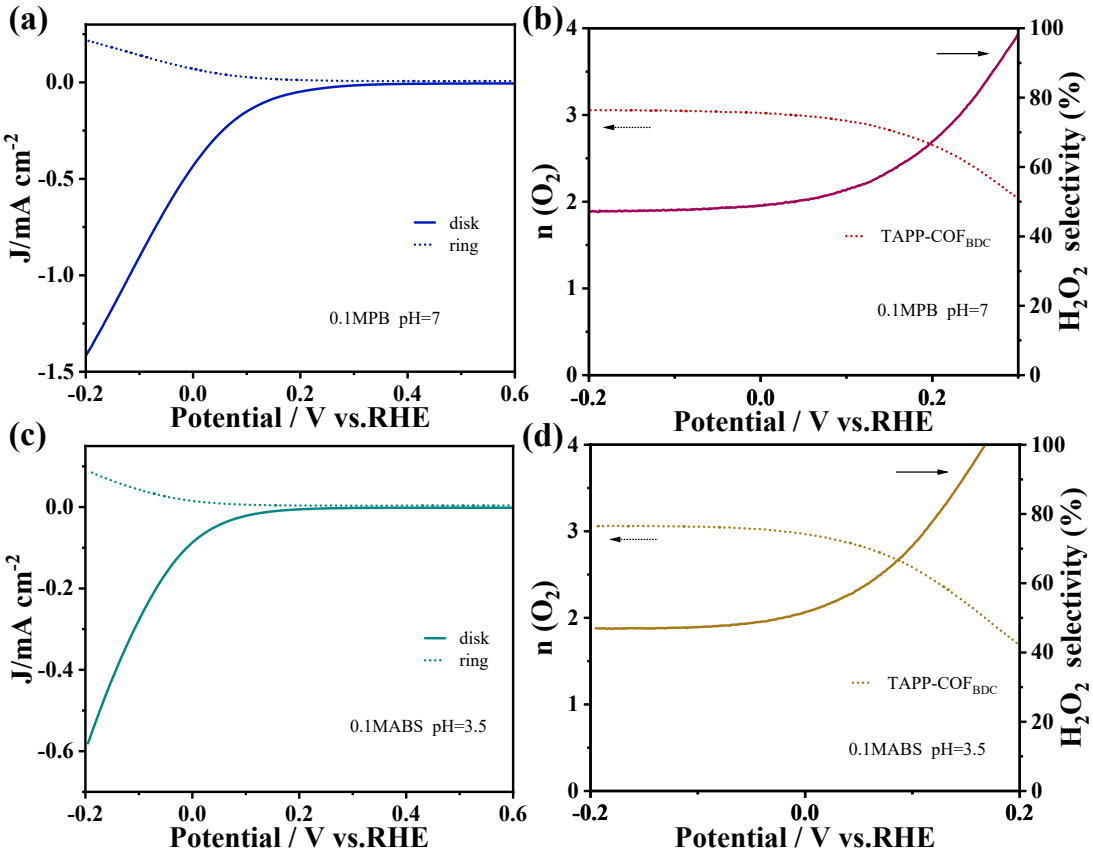

Figure S6. RRDE LSV polarization curves of TAPP-COF_{BDC} in O_2 saturated 0.1 M PB (pH = 7.0) (a) and 0.1 M ABS (pH = 3.5) (c) electrolytes. Calculated electron transfer number n and the H_2O_2 selectivity (b, d).

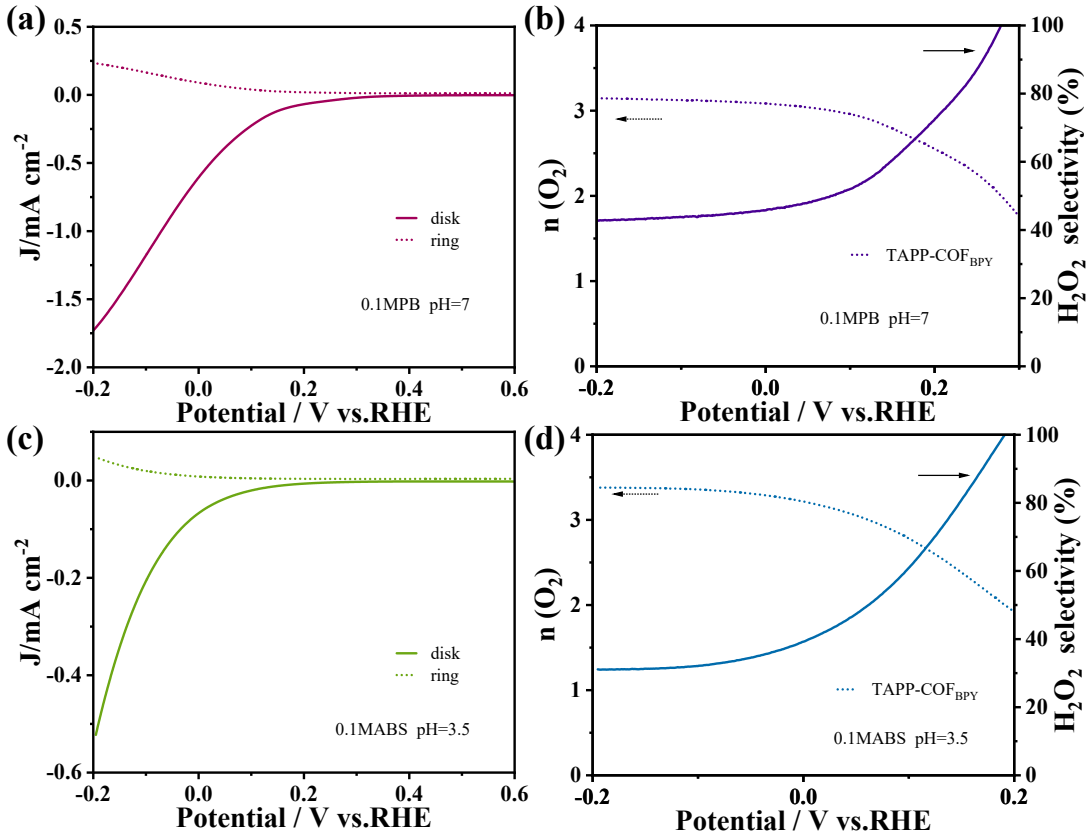

Figure S7. RRDE LSV polarization curves of TAPP-COF_{BPY} in O_2 saturated 0.1 M PB (pH = 7.0) (a) and 0.1 M ABS (pH = 3.5) (c) electrolytes. Calculated electron transfer number n and the H_2O_2 selectivity (b, d).

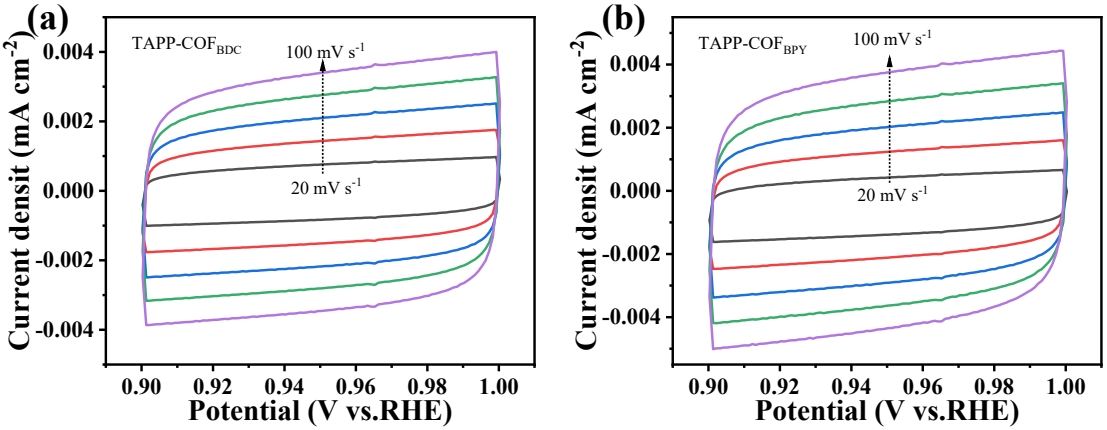

Figure S8. Cyclic voltammogram in the non-faradic potential region at varying scan rates (a) TAPP-COF_{BDC} and (b) TAPP-COF_{BPY}.

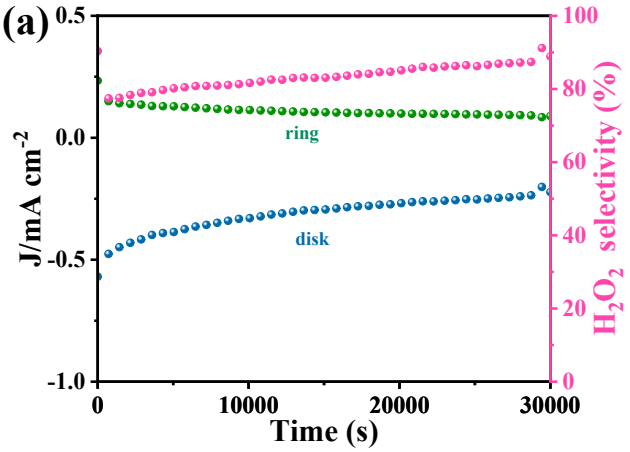

Figure S9. Chronoamperometry measurement of the TAPP-COF_{BDC} for 30000 s at 0.6 V vs RHE.

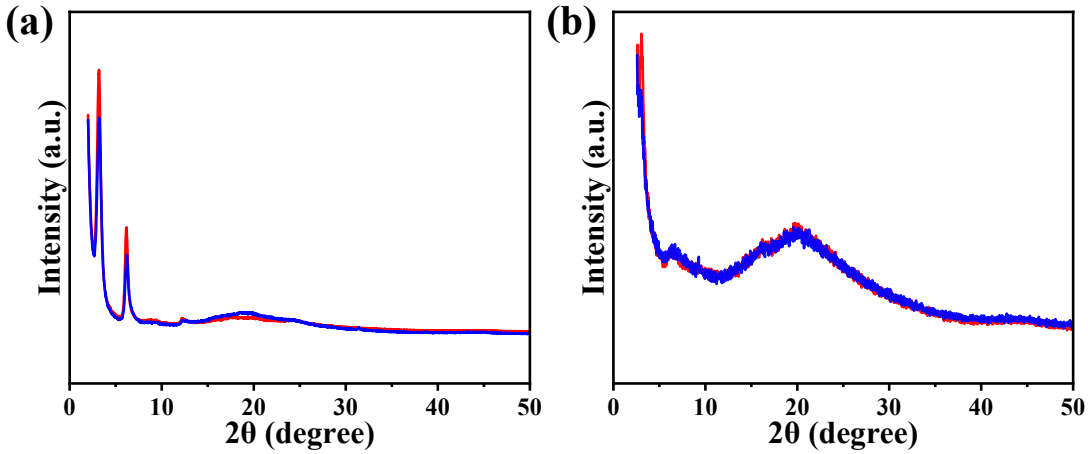

Figure S10. Chemical stability of TAPP-COF_{BDC} (a) and TAPP-COF_{BPY} (b). The pristine (red) and after 30000 s treatment under KOH (0.1 M, blue) at room temperature.

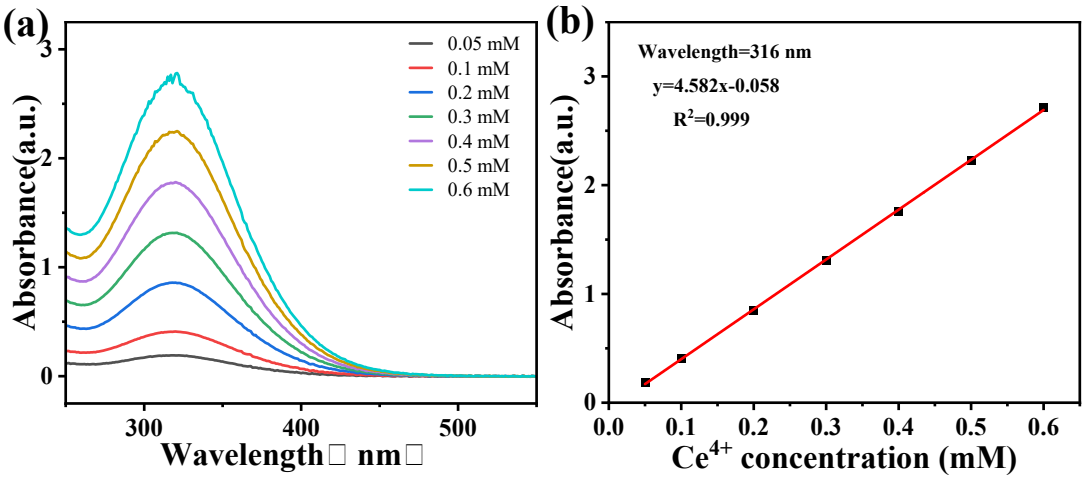

Figure S11. (a) UV/visible absorption spectra of Ce^{4+} at different concentrations, (b) The relationship between Ce^{4+} concentration at 316 nm and absorbance.

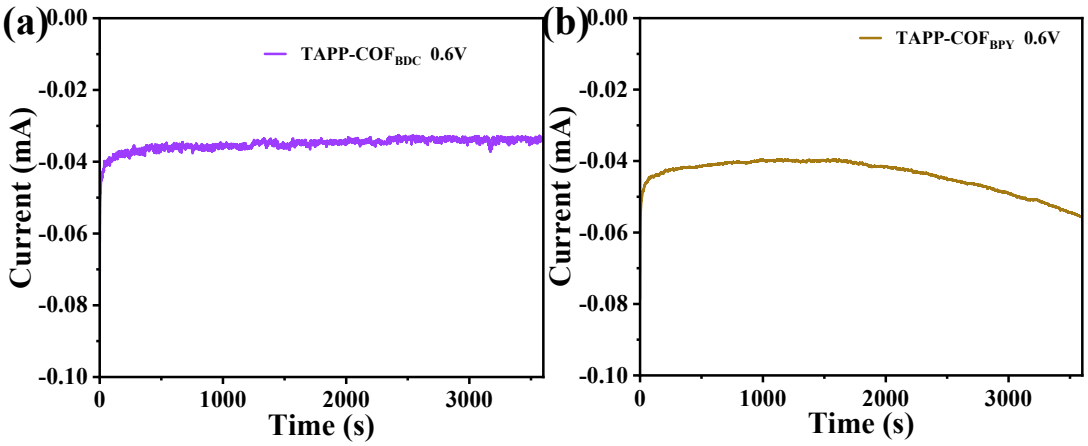

Figure S12. H_2O_2 electroproduction in the H-cell flow cell with 0.1 M KOH electrolyte. The chronoamperometry measurements at 0.6 V vs RHE. of (a) TAPP-COF_{BDC} and (b) TAPP-COF_{BPY}.

Table S1. The comparison of reported COFs toward electrocatalytic 2e- ORR for H_2O_2 production

Catalysts	Maximum Selectivity by RRDE (%)	H_2O_2 production rate (mmol g^{-1} h^{-1})	Faradaic efficiency(%)	ref
TAPP-COF_{BDC}	76	5.6 (0.6 V vs. RHE)	86	This work
TAPP-COF_{BPY}	88	7.4 (0.6 V vs. RHE)	90	
Ca-COF-318	95	453 (mmol cm^{-2} h^{-1}) (0.4 V vs. RHE)	91	Chem.-Asian J., 2021, 16, 498-502
PYTA-TPEDH-COF	85.8	-	80	Small, 2022, 18, 2204757
COF-366-Co	91	909 (250 mA)	84	J. Am. Chem. Soc., 2020, 142, 21861-21871
O-HATP-HKH-CON	99.6	0.139 (0.2 V vs. RHE)	93	Angew. Chem. Int. Edit., 2023, 62, e202218742
Br-COF	86.2	-	80.6	Appl. Catal. B Environ., 2021, 298, 120605
DFTAPB-TFTA-COF/GC	96.25	-	71.1	Appl. Catal. B Environ., 2024, 344, 123611
TAPB -TA - COF/GC	44.7	-	28.7	
TAE-COF	98.2	8500 (50 mA/cm^2)	73	Angew. Chem. Int. Edit., 2023, 62, e202313940
PYTA-PTDE-In	80	180.4 (0.2 V RHE)	76	Acs Appl. Mater. Inter., 2024, 16, 56459-56468
PYTA-PTDE-Sn	90	148 (0.2 V RHE)	80	
PYTA-PTDE-Sb	96	209.2 (0.2 V RHE)	90	
Py-Bpy-COF-Zn	99.1	9278 (40 mA cm^{-2}; Flow cell）	-	Chem. Comm., 2023, 59, 10424-10427
JUC-660	86	1398 (40 mA cm^{-2}; Flow cell）	83.6	Angew. Chem. Int. Edit., 2024, 63, e202410417
Py-TD-COF	92	218 (0.55V vs. RHE)	-	Susmat, 2023, 3, 379-389
Py-TD-COF-NH	61	-	-	

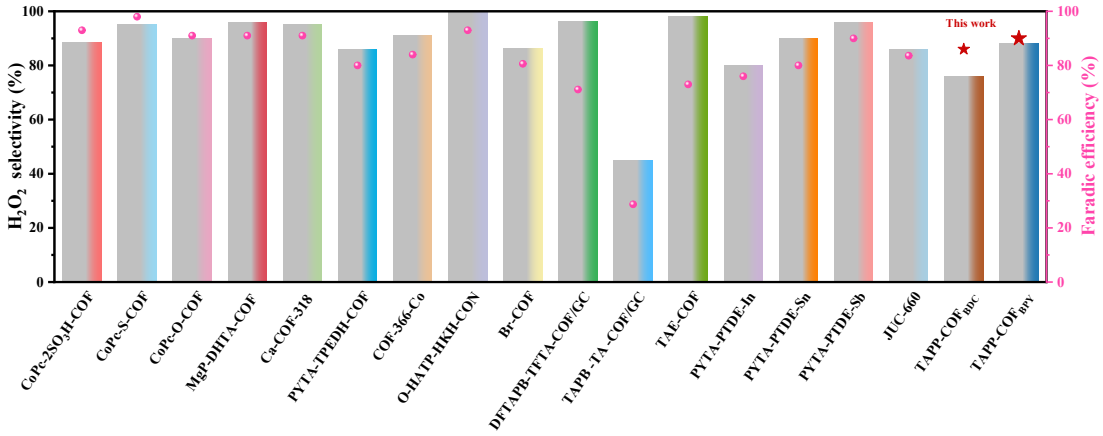

Figure S13. Comparison of H_2O_2 selectivity and faraday efficiency of H_2O_2 formation in different COF-based catalysts by ORR.

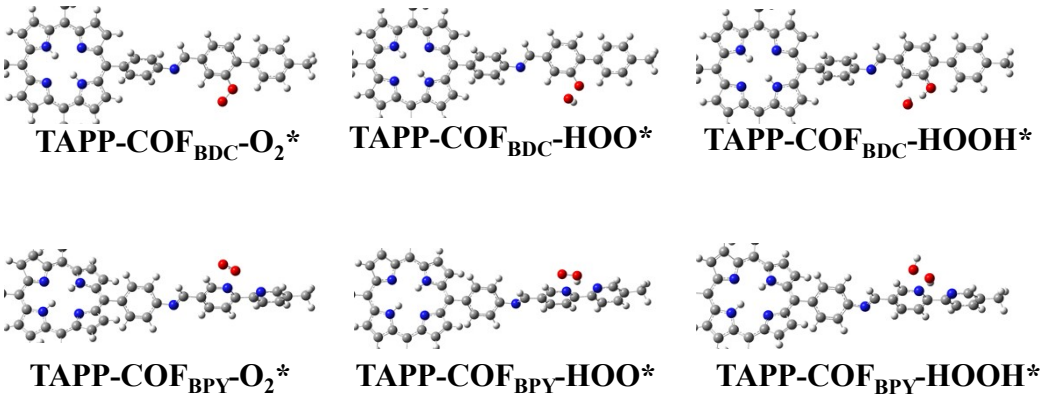

Figure S14. The schematic mechanism for ORR of COFs

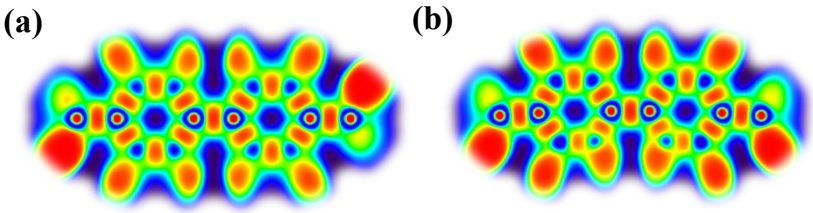

Figure S15. Electronic cloud distribution of TAPP-COF_{BDC} and TAPP-COF_{BPY}

Section 5. Theoretical calculations

The free energy of the adsorbed state (ΔG) was calculated using the Gaussian 09W program. During geometry and frequency optimization, all atoms were allowed to move freely. Based on the Density Functional Theory (DFT), the quantum cluster calculations were carried out using the B3LYP/6–31G (d, p) basis set. The SMD solvation model was used to consider the solvent (water) effect. The free energy were calculated by the equation:

$$\Delta G_H = \Delta E_{ad} + \Delta E_{ZPE} - T\Delta S \quad \text{(S9)}$$

Here, E_{DFT} represents the total energy calculated using Density Functional Theory (DFT), E_{ZPE} is the zero-point energy correction. Additionally, ΔE is the electronic energy difference obtained directly from DFT calculations, and ΔE_{ZPE} is the change in zero-point energy.

$$T\Delta S = \Delta H - \Delta G \quad \text{(S10)}$$

ΔH is thermal correction to Enthalpy, ΔG is thermal correction to Gibbs Free Energy.

References

1. A. Bettelheim, B. A. White, S. A. Raybuck and R. W. Murray, Inorg. Chem., 1987, **26**, 1009-1017.
2. C. J. Wu, X. Y. Li, M. Z. Shao, J. L. Kan, G. B. Wang, Y. Geng and Y. B. Dong, Chinese Chem. Lett., 2022, **33**, 4559-4562.
3. L. J. Gong, L. Y. Liu, S. S. Zhao, S. L. Yang, D. H. Si, Q. J. Wu, Q. Wu, Y. B. Huang and R. Cao, Chem. Eng. J., 2023, **458**, 141360.